Quantitative Transduction of Excited-State Energy in Fluorophore-Heterofullerene Conjugates

Frank Hauke,[a] Andreas Hirsch,*[a] Stefan Atalick,[b] and Dirk Guldi*[b,c]

Keywords: Fullerenes / Heterofullerenes / Fluorophores / Energy transfer / Quantum chemistry

A novel series of fluorophore-heterofullerene conjugates **10**–**14** – the fluorophores range from benzene, naphthalene, phenanthrene, and fluorene to pyrene – was synthesized. NMR spectroscopy and quantum mechanical calculations demonstrate that the flexibility of the acetyl-group linker opens the way for conformations with π–π stacking interactions between the chromophores. This leads to favorable electronic communication between the two subsystems and is reflected in a series of ground- and excited-state assays ranging from fluorescence to fast transient absorption measurements. It was found that a common deactivation process of the photoexcited fluorophores takes place, namely, a quantitative transduction of singlet excited state, yielding the heterofullerene singlet excited state. This reaction pathway leads to the long-lived and highly reactive fullerene triplet state, which forms, in a reaction with molecular oxygen, a cytotoxic oxygen species (i.e. singlet oxygen).

Introduction

The initial event in bacterial photosynthesis involves the absorption of photons by the light-harvesting antenna system, which is followed by a rapid transduction of this energy − over large distances and in high quantum yields − to the reaction centre protein, where "electron transfer" trapping occurs.[1] However, owing to the complex requirements that are associated with sequential energy and electron transfer relays, optimization of each individual step involved becomes central. In this respect, free energy changes, electronic couplings and spectral overlaps are three of the most important parameters gauging the rates and efficiencies of electron- and energy-transfer processes.[2] Additionally, energy-transfer processes in a cascade like arrangement are the focus of efficient light conversion into states that are longer-lived than the precursor excited states. An alternative motivation is the biologically important production of singlet oxygen ($^1O_2$) as a product of excited-state quenching.[3,4]

Fullerenes have proven to be a rich platform for conducting supramolecular and nanoscale chemistry,[5,6] which allows, for example, the design of architectures that are suitable for undergoing photoinduced electron- and energy-transfer processes. Covalent functionalization of the fullerene core[6] with fluorophore moieties is expected to enhance the ground-state absorption of the resulting dyads and is expected to promote the light-harvesting effect. As fluorophore substituents we have chosen polycyclic aromatics, not only because they are often used as chromophores, but also due to their high-lying excited states and their strongly fluorescing features.

Integrating several redox- and light-responsive systems into a single ensemble requires careful adjustment of the properties of the individual components and their optimization. An attractive alternative to isocyclic fullerenes, as components for such conjugates, are hetereofullerene building blocks (i.e. $C_{59}N$).[7] We have recently developed a variety of versatile protocols for the direct and completely regioselective attachment of aromatic as well as aliphatic moieties, namely, adjacent to the hetereoatom.[8] In such azaheterofullerene derivatives, substitution of a carbon atom with nitrogen alters the redox potential and the excited-state energies of the fullerene.[9] Significantly, $C_{59}N$ derivatives render better electron acceptors than C_{60} and C_{60} derivatives that bear similar addends. We are interested in accomplishing a better understanding of factors that govern and optimize electron and energy transduction processes in $C_{59}N$-based donor-acceptor conjugates en route to integrated devices for solar energy conversion.

Here we describe the synthesis of a series of heterofullerene-fluorophore conjugates and the dynamics of the individual processes following photoexcitation by means of transient spectrophotometric and fluorometric techniques (Figure 1). We believe that this approach offers a viable al-

[a] Institut für Organische Chemie,
Henkestrasse 42, 91054 Erlangen, Germany
Fax: +49-9131-852-6864
E-mail: hirsch@organik.uni-erlangen.de
[b] Radiation Laboratory, University of Notre Dame,
IN 46556, USA
Fax: +1-219-631-8068
E-mail: guldi.1@nd.edu
[c] Institut for Physical Chemistry,
Egerlandstrasse 3, 91085 Erlangen, Germany
Fax: +49-9131-852-8307
E-mail: dirk.guldi@chemie.uni-erlangen.de

 DOI: 10.1002/ejoc.200400771

ternative for developing well-defined architectures, bearing a $C_{59}N$ core, which give rise to sequential energy and electron transduction processes.

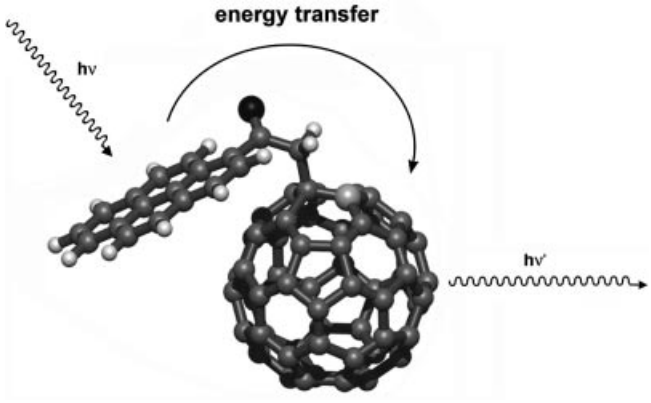

Figure 1. Schematic representation of the interaction of heterofullerene-fluorophore conjugates after excitation of the acceptor subunit.

Results

Synthesis of the Heterofullerene-Fluorophore Conjugates

Substituting a single carbon atom of the C_{60} framework with nitrogen leads to the formation of an open-shell system. Consequently, the simplest azaheterofullerene can only be isolated as its corresponding dimer **1**.[7] In the dimeric form two $C_{59}N$ moieties are connected through an sp^3-carbon adjacent to the nitrogen.

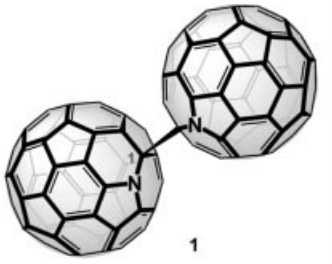

1

In conventional donor-acceptor dyads, which involve the isocyclic C_{60} core, cycloaddition reactions of either linker molecules or donor components take place at a [6,6]-double bond of the fullerene core. Since all [6,6]-double bonds of C_{60} are topologically identical, only one regioisomer is formed during the monoaddition reaction. In the case of $(C_{59}N)_2$ (**1**), topologically and chemically different [6,6]-double bonds are present. Consequently, several regioisomeric cycloadducts might be formed. The chemistry of $(C_{59}N)_2$ (**1**), on the other hand, is characterized by an interfullerene bond that is subject to thermal cleavage. The resulting open shell $C_{59}N$ radical or its oxidation product $C_{59}N^+$ undergoes saturation through the addition of a radical or a nucleophile.[7–9] Following both reaction paths only monoadducts are formed, in which the addends are always located at the C-1 position, namely, adjacent to the heteroatom. Based on the $C_{59}N^+$ chemistry,[8,10] direct attachment of an aromatic (i.e. serving as the trapping nucleophile itself – *type 1*)[8a] and/or indirect attachment (i.e. through an enolizable side chain – *type 2*)[8b–8d] are conceptually possible. In the first case, rigid molecular architectures are obtained, in which the aromatic moiety is directly connected to the heterofullerene core. We have recently described the syntheses and the physical properties of this kind of heterofullerene derivatives emerging from the connection of the $C_{59}N$ core and coronene, pyrene, corannulene, and ferrocene.[11]

By inspecting, for instance, 1-(hydroazafullerenyl)pyrene (**2**)[11a] (Figure 2), the only conformational freedom involves rotation of the addend about the connecting σ bond. The π orbitals of the arene subunit and that of the heterofullerene core assume perpendicular orientations to each other. Therefore, the electronic communication between the redox-active moieties is less than perfect. Nevertheless, a quantitative transduction of photonic excited-state energy from the arene subunit to the azaheterofullerene core is observed. This is a promising result for the systems investigated in this study.

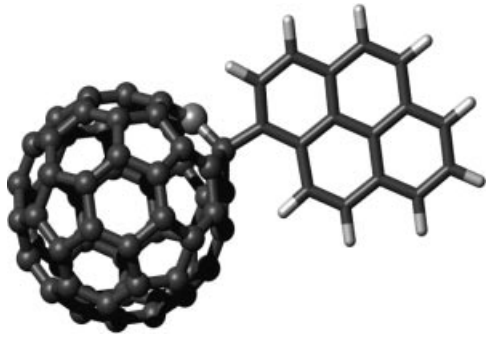

Figure 2. Rigid structure of 1-(hydroazafullerenyl)pyrene (**2**).

The introduction of an aliphatic linker between the fullerene core and the arene moieties will further enhance the flexibility. It should then be possible to orientate the two different π systems so that an optimal overlap between the two sets of orbitals is achieved. Therefore, the electronic coupling in these conjugates should be better than in the rigid system **2**. For the construction of such architectures we chose the *type 2* functionalization method.[8b–8d] As starting materials we used the acetyl-substituted aromatics **3**–**7**, which led to the introduction of a flexible $–CH_2CO–$ linker after coupling with the $C_{59}N$ moiety. The selection of fluorophores **3**–**7** allows for the modulation of the absorption cross sections within the range of 300 to 400 nm. Furthermore, the C_2 acetyl linker ensures that all different fluorescent subunits have the same spatial distance relative to the heterofullerene core and the same degree of rotational freedom. Therefore, the photophysical properties can be directly related to the fluorophore–heterofullerene interactions. The syntheses were carried out by treating **1** with the corresponding acetyl fluorophores **3**–**7** and *p*-TsOH at 150 °C in *o*-dichlorobenzene (ODCB) under a constant stream of air. The resulting fluorophore-heterofullerene conjugates **10**–**14** were obtained in good yields. Compound

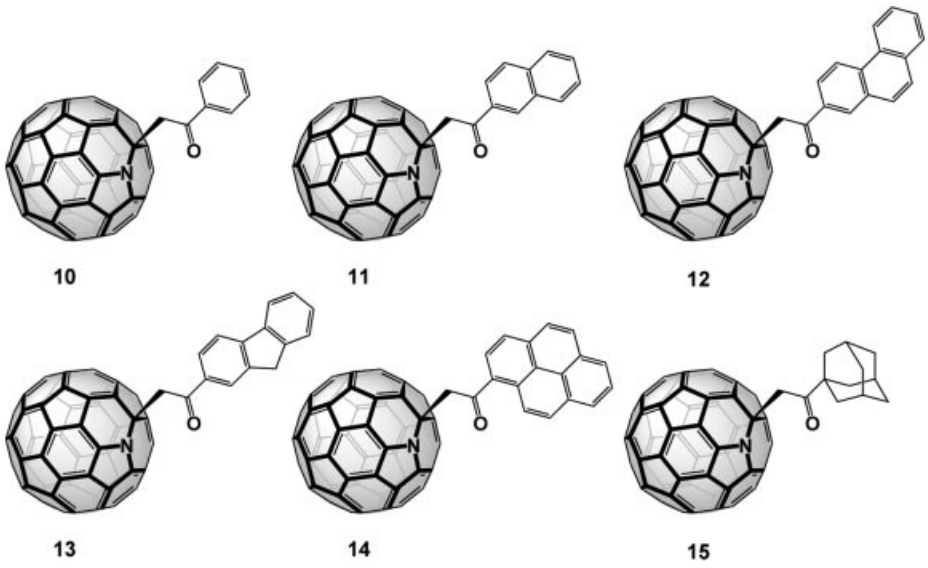

15, carrying a non-aromatic adamantyl addend, was prepared for comparison. The complete structural characterization of adducts **10**–**15** was carried out by ^{1}H NMR, ^{13}C NMR, UV/Vis, and FT-IR spectroscopy as well as by mass spectrometry.

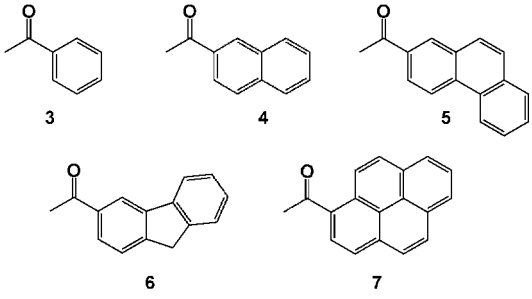

Spatial Orientation of the Subunits

In general, a pronounced back folding tendency of the extended π moiety towards the heterofullerene core is deduced from the analysis of the ^{1}H NMR spectra of conjugates **10**–**14**. In the following, we would like to demonstrate this by discussing the 1-acetyl pyrene-heterofullerene adduct **14**. If, in fact, the steric demand of the substitutions would be the only factor governing the adoption of the most preferred conformation, we would expect an antiperiplanar orientation of the pyrene substituent relative to the heterofullerene core. This scenario is illustrated in Figure 3. In this conformation, the repulsive interaction between the substituent and fullerene is minimal.

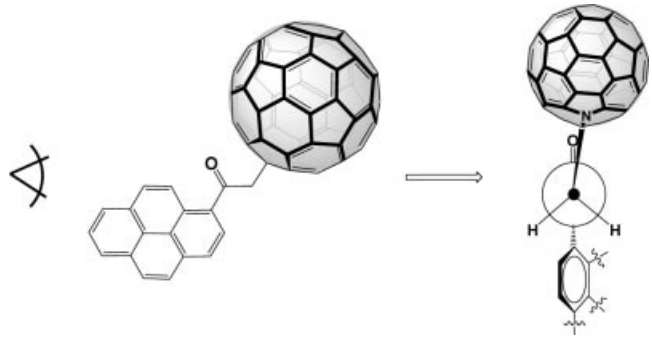

Figure 3. Preferential orientation of the subunits taking into account steric effects only.

In this case, the anisotropic influence of the heterofullerene π-system on the chemical shifts of the pyrene protons should be weak, because the two subsystems are spatially separated. An attractive π–π interaction between the two subunits, on the other hand, should lead to the back folding of the pyrene substituent towards the heterofullerene core. This situation is shown in Figure 4, where the antiperiplanar conformation is superimposed with the conformation that accounts for the efficient π–π stacking interaction. The closest distance that spans between the fullerene surface and the protons on the pyrene ring is about 3.2 Å (semiempirical calculations with PC-Spartan Pro[12]), compared to 5.2 Å in the antiperiplanar conformation. In **2**,[11a] where the pyrene unit is directly connected to the heterofullerene core, the closest distance to the arene protons is only 2.0 Å. The ^{1}H NMR spectrum of **2** reveals large anisotropic shifts for the resonances related to the pyrene protons. Figure 5 shows a direct comparison of the ^{1}H NMR spectrum of pyrene (**19**) and 1-(hydroazafullerenyl)pyrene (**2**).

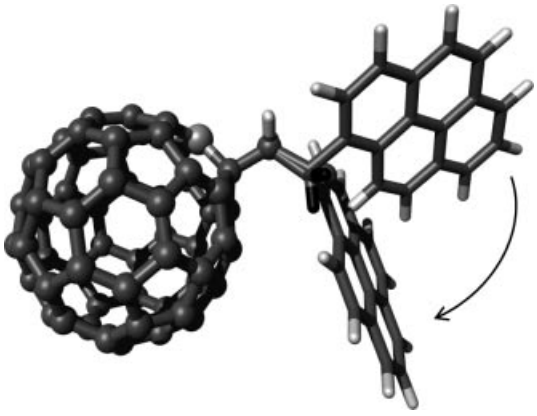

Figure 4. Schematic representation of the back folding of the pyrene moiety (**14**).

The doublet located at δ = 10.53 (^3J = 9.4 Hz) corresponds to proton H1, which has the shortest distance (2.04 Å) to the heterofullerene surface. The signal of this proton is shifted by 2.43 ppm downfield, due to the anisotropic influence of the fullerene core. The doublet at δ = 9.54 (^3J = 8.2 Hz) can be traced back to H9 with a distance of 2.41 Å in relation to the fullerene surface. This proton experiences an anisotropic shift of 1.33 ppm. The downfield shift of proton H8 (δ = 8.57, doublet, ^3J = 8.2 Hz) and H2 (δ = 8.51, doublet, ^3J = 9.4 Hz) is 0.48 ppm and 0.38 ppm, respectively. H9 is 4.02 Å and H3, 4.61 Å away from the π surface of the fullerene. The increased spatial distance between the remaining protons and the heterofullerene core leads only to small anisotropic shifts. The assignment of the signals was carried out by using H-H-COSY and C-H-COSY spectroscopy. The distances have been determined from the geometric optimized PM3 structures.[12] These investigations clearly demonstrate that heterofullerene-acetyl arene conjugates **10**–**14** adopt antiperiplanar conformations (Figure 3) and involve a spatial separation of the closest arene proton from the fullerene surface of about 5.2 Å only. As a consequence, only very weak anisotropic shifts are to be expected. However, this is not the case. Figure 6 compares the ^{1}H NMR spectra of 2-acetylpyrene (**7**) and 2-(hydroazafullerenyl)-1-(pyren-1-yl)ethanone (**14**). Again, a significant downfield shift of the signals for the arene protons is observed. Proton H1 experiences the biggest downfield shift (δ = 0.68). Its doublet (^3J = 8.0 Hz) appears at δ = 9.00. Proton H9 (δ = 9.51, ^3J = 9.3 Hz) and proton H8 (δ = 8.39, ^3J = 8.0 Hz) experience a downfield shift of 0.45 and 0.23 ppm, respectively. Even the triplet of proton H6 (δ = 8.10, ^3J = 7.7 Hz), which has the largest distance to the acetyl function, is shifted downfield by 0.12 ppm. Again, the signal assignment was carried out by using H,H-COSY and C-H-COSY spectroscopy.

The downfield shifts of the arene protons are mainly due to the anisotropic influence of the heterofullerene core. The –I effect of azaheterofullerenes should play no crucial role, since the fullerene moieties and arene subunits are separated by C_2 spacers. We conclude that a low-energy conformer is preferred, in which attractive π–π interactions leads to a back folding of the arene moiety towards the fullerene surface. In this conformer, the π systems of both chromophores are oriented parallel to each other (Figure 4). As a consequence, favorable electronic through-space interactions between the two redox-active moieties are enabled. However, at room temperature rotation about the σ bonds within the dyads **10**–**15** is still allowed. This is exemplified in the ^{13}C NMR spectra of all heterofullerene conjugates **10**–**15**, which all reveal C_s symmetry. Therefore, the rotations are fast on the NMR time scale. The signals for the aromatic moieties and those for the sp^2 signals of the heterofullerene core are located in the region between δ = 158 and δ = 110. Comparison of these signals with those of the parent arenes helps to analyze the $C_{59}N$ resonances from the sp^2 signals of the aromatics. Altogether 30 signals – in the region between δ = 158 and δ = 120 – correspond, therefore, to the fullerene sp^2-C atoms. Twenty eight of these signals show double intensity and two of them

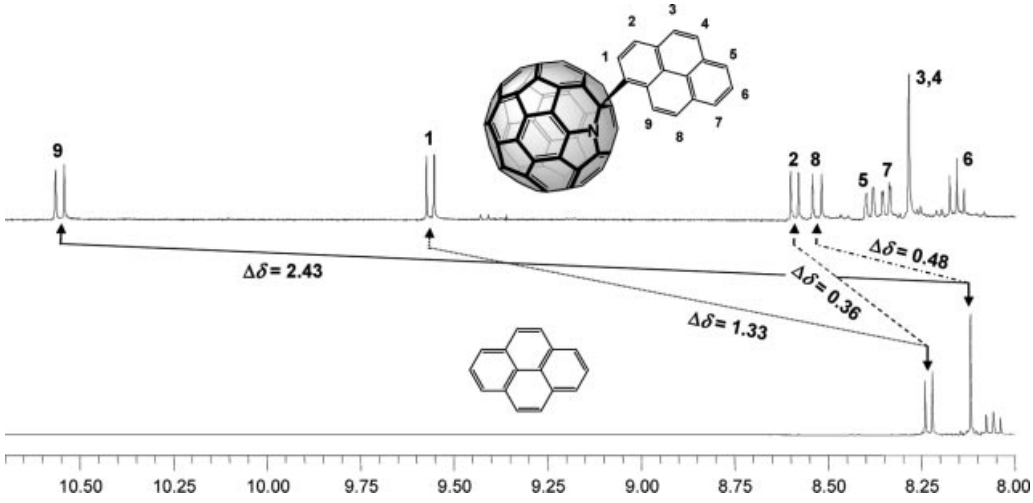

Figure 5. 400 MHz ^{1}H NMR spectrum (CS_2/$CDCl_3$) of pyrene (**19**) [bottom] and 1-(hydroazafullerenyl)pyrene (**2**) [top].

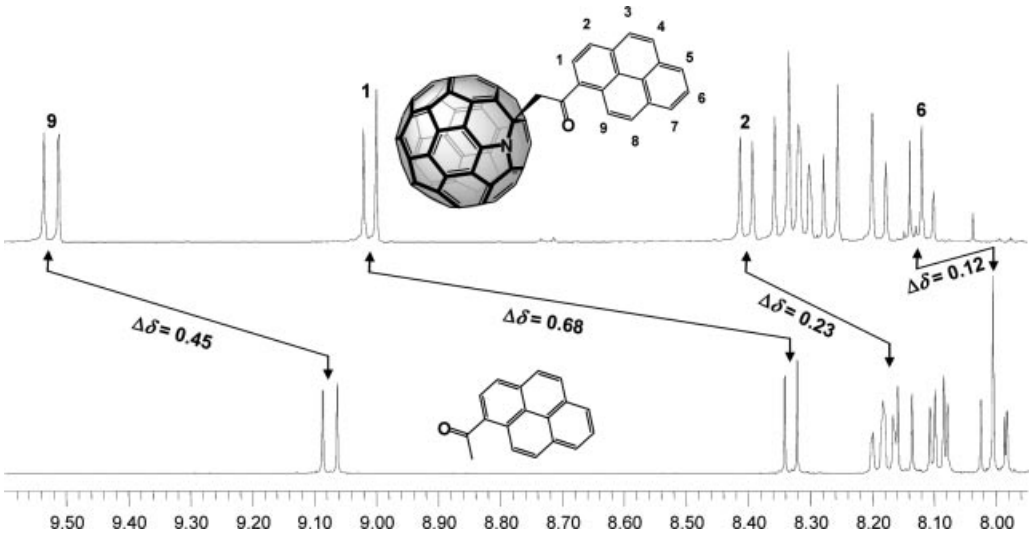

Figure 6. 400 MHz ^{1}H NMR spectrum (CS_2/$CDCl_3$) of 1-acetylpyrene (**7**) [bottom] and 2-(hydroazafullerenyl)-1-(pyren-1-yl)ethanone (**14**) [top].

show single intensity. The latter belong to the fullerene *trans*-1 carbon atoms, located on the mirror plane. The characteristic signal of the sp^2-C atom of the heterofullerene cage appears in the region between δ = 85 and δ = 89. In conclusion, the NMR spectra of **10**–**14** clearly show that these dyads are rather flexible. However, confirmations involving effective π–π stacking interactions between the chromophores are preferred.

Ground-State Features

As mentioned above, the selection of fluorophores **3**–**7** allows for the modulation of the absorption cross sections within the range 300–400 nm. As far as exploring possible electronic perturbations in the singlet ground state is concerned, it is important to gather that the ground-state absorption spectra of all fluorophore-heterofullerene conjugates **10**–**14** appear as nearly strict superimpositions of those of the individual fragments, **3**–**7** and $C_{59}N$ reference **20**. This indicates the absence of strong interactions between $C_{59}N$ and the different fluorophores.

Excited-State Features

In the next step we tested the excited-state interactions in fluorophore-heterofullerene conjugates (**10**–**14**) by means of steady-state and time-resolved photolytic experiments, including fluorescence and transient absorption measurements. In particular, the photophysics of **10**–**15** were compared with i) two sets of suitable fluorophore references, that is, pristine compounds **16**–**19** (Figure 7) and their acetyl analogues **3**–**7** and ii) $C_{59}N$ reference **20**.

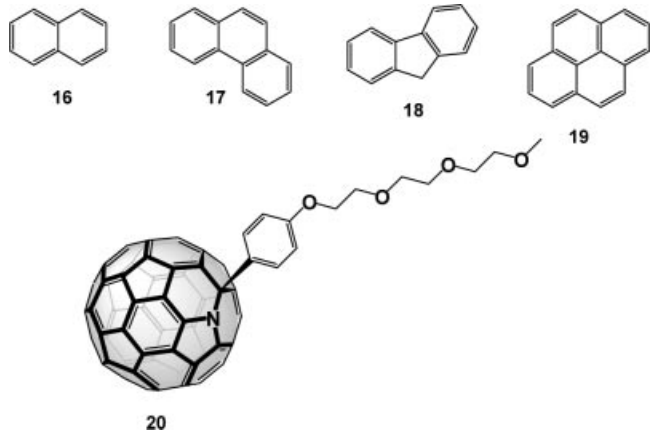

Figure 7. Fluorophore reference compounds **16**–**20**.

Steady-State Fluorescence

As a general feature, the fluorescence spectra of **3**–**7**, **10**–**15**, **16**–**19**, and **20** should be discussed by dividing them into two sections. First, the high-energetic near-visible region should be considered where, typically, the strong fluorophore emission is detected. Second, the low-energetic near-infrared part emerges, where the $C_{59}N$ emission[9h] is expected to be seen. An illustration is given in Figure 8, which summarizes the differences between the fluorophore (**19**) emission features and that of $C_{59}N$ derivative **20**.

All fluorophore references **16**–**19** are extremely strong singlet excited-state emitters, with quantum yields that approach unity.[13] This renders them convenient probes for the photophysical measurements, especially regarding intramolecular interactions in the fluorophore-heterofullerene conjugates. In the set of acetyl references **3**–**7**, the light emission is, however, significantly lower. The difference, for example, in the pyrene derivatives is as great as 350. An

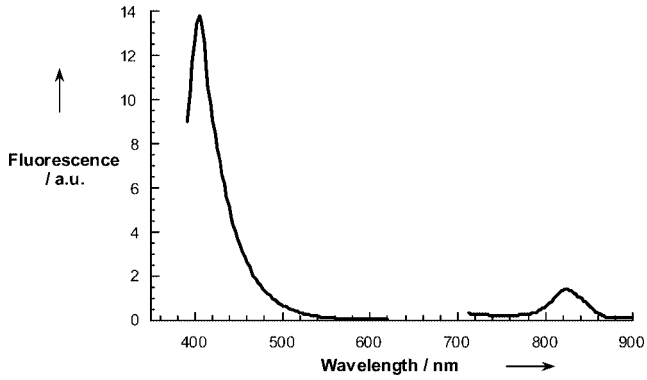

Figure 8. Fluorescence spectra of **19** and **20** displayed in the regions 380–620 and 720–900 nm, respectively, following 350 nm photoexcitation. Please note that the fluorescence intensity is arbitrary in these cases.

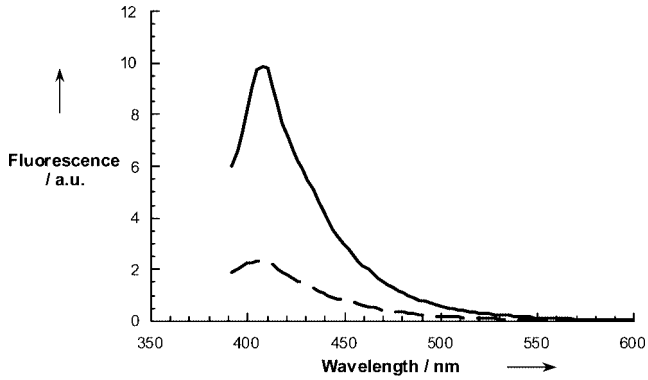

Figure 9. Fluorescence spectra of 1-acetylpyrene (**7**) (solid line) and 2-(hydroazafullerenyl)-1-(pyren-1-yl)ethanone (**14**) (dashed line) in toluene with matching absorption at the 350 nm excitation wavelength – OD_{350nm} = 0.8.

important structural aspect is that the fluorophores **3**–**7** bear acetyl functionalities, which makes them a priori weaker emitters than typically found for the analogous pristine materials **16**–**19**. A likely rationale can be sought in the dominating n-π* character of the acetyl functionalities, rather than just being a pure π-π* state. The impact of the n-π* character is so strong that its presence leads to a decrease in the radiative (i.e. fluorescence) and an increase in the nonradiative contribution (i.e. intersystem crossing) for the deactivation of photoexcited **3**–**7**.

Despite the highly constrained and rigid carbon network in fullerenes, their singlet excited states give rise to a surprisingly weak emission, and $C_{59}N$ derivative **20** is no exception to that trend. Its fluorescence quantum yield (Φ) is quite moderate with a value of 1.5×10^{-4}.[9h] For **20**, it holds that when comparing its room temperature emission with a low-temperature experiment a significant gain of resolution is realized. At 77 K, **20** exhibits maxima at 815, 828, and 833 nm, while at room temperature only a single *0–0 emission peak is noted at 825 nm.

In a typical fluorescence experiment performed with fluorophore-heterofullerene conjugates **10**–**14**, the ground-state maxima of the fluorophores (i.e. 318–390 nm) were chosen as the excitation wavelength to ensure quantitative excitation of the fluorophore. Typically, less than 10% of the excitation light reaches the $C_{59}N$ moiety. Variable extents of fluorophore emission quenching are noted in **10**–**14** (see Figure 9).

Table 1 reveals that the quenching ratio ranges from 3 to 1100. Interestingly, while the quenching is quite drastic in relation to **16**–**19** with factors as large as 1100, it is as little as 3 relative to some of the acetyl references **3**–**7**. It is important to note that even under the latter circumstance, that is, n–π* induced deactivation of the fluorophore fluorescence, additional quenching is still discernible.

Analogous with the fluorophore quenching in the near-visible region (Figure 9), we found a new emission band in the near-infrared region (Figure 10): maxima at around 825 nm are characteristic of the $C_{59}N$ fluorescence. Considering that the fluorophores were excited at their ground-state maxima, where the $C_{59}N$ contribution is marginally small (i.e. less than 10%), the transfer of singlet excited-state energy is very likely to be responsible for the $C_{59}N$ fluorescence.

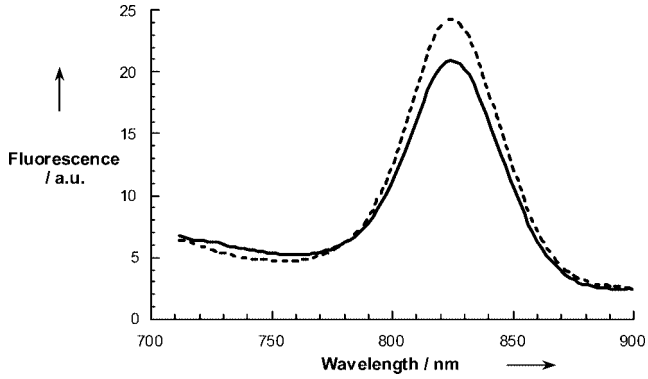

Figure 10. Fluorescence spectra of $C_{59}N$ derivative **20** and 2-(hydroazafullerenyl)-1-(pyren-1-yl)ethanone (**14**) (dashed line) in toluene with matching absorption at the 350 nm excitation wavelength – OD_{350nm} = 0.8.

To confirm the origin of the near-infrared fluorescence, an excitation spectrum of the 825 nm emission was taken. For example, 2-azafullerenyl-1-(1-pyrenyl)ethanone (**14**) and 1-acetyl pyrene (**7**) both reveal identical excitation maxima at around 390 nm, which also matches the maximum of the pyrene ground-state absorption in **7** and **14**. Similar observations were made for the remaining fluorophore-heterofullerene conjugates.

To quantify the energy transfer efficiency in **10**–**14**, the $C_{59}N$ fluorescence quantum yields were determined with reference to a suitable model compound, **20**, with matching absorption at the excitation wavelength. As can be seen by inspection of Table 1, the quantum yields in toluene are close to 1.5×10^{-4} and confirm a nearly quantitative transfer. A complementary set of experiments in a more polar solvent such as *o*-dichlorobenzene led to the same results. The latter data are important, since it proves that energy transfer is the main process by which the photoexcited

Table 1. Photophysical properties of **3**–**7**, **10**–**15**, **16**–**19** at room temperature.

	Benzene (320 nm)	Adamantane (318 nm)	Fluorene (318 nm)	Naphthalene (342 nm)	Phenanthrene (368 nm)	Pyrene (390 nm)
			17	**16**	**18**	**19**
Fluorescence maximum		broad UV emission	342 nm (3.62 eV)	339 nm (3.65 eV)	369 nm (3.35 eV)	396 nm (3.12 eV)
Fluorescence quantum yield	0.06		0.7	0.2	0.18	0.72
Fluorescence lifetime	30 ns	81 ns 14 ns/oxygen	8 ns 3 ns/oxygen	90 ns 19 ns/oxygen	55 ns 15 ns/oxygen	260 ns 19 ns/oxygen
Triplet maxima		360 nm	390 nm	410 nm	480 nm	420 nm
Triplet lifetimes			150 μs	50 μs	95 μs	180 μs
	3		**6**	**4**	**5**	**7**
Fluorescence maximum	362 nm (3.42 eV)	356 nm (3.48 eV)	352 nm (3.52 eV)	385 nm (3.2 eV)	411 nm (3.01 eV)	406 nm (3.05 eV)
Fluorescence quantum yield	0.001	0.002	0.0018	0.0005	0.001	0.0021
Fluorescence lifetime		0.14 ns	0.2 ns	0.19 ns	0.23 ns	0.15 ns
Triplet maxima	360 nm	360 nm	440 nm	420 nm	500 nm	440 nm
Triplet lifetimes	0.5 μs	3 μs	15 μs	3 μs	9 μs	15 μs
	10	**15**	**13**	**11**	**12**	**14**
Fluorescence quantum yield (i.e. fluorophore)	0.0003	0.00035	0.0004	0.00013	0.00014	0.00064
Fluorescence lifetime (i.e. fluorophore)	0.11 ns	0.13 ns	0.13 ns	0.1 ns	0.1 ns	
Fluorescence quantum yield (i.e. $C_{59}N$)	1.0×10^{-4}	0.96×10^{-4}	0.91×10^{-4}	0.96×10^{-4}	0.84×10^{-4}	0.96×10^{-4}
Fluorescence lifetime (i.e. $C_{59}N$)	1.1 ns	1.1 ns	1.2 ns	1.1 ns	1.2 ns	1.0 ns
Triplet quantum yield (i.e. $C_{59}N$)	100%	98%	88%	89%	94%	97%
Triplet lifetimes (i.e. $C_{59}N$)				15 μs		

fluorophores deactivate in **10**–**14**. Electron transfer, on the other hand, which is expected to become more exothermic in the more polar solvents, plays no relevant role.[14]

Time-Resolved Fluorescence

Time-resolved emission experiments allow us to analyze the contributions from both fragments, that is, the near-visible fluorophore fluorescence and the near-infrared $C_{59}N$ fluorescence. Therefore, following the 337 nm laser excitation, the fluorescence decay was probed in both regions.

Let us first address the question of the fluorophore emission in the two sets of reference compounds, **16**–**19** and **3**–**7**. The acetyl functionality has a strong impact on the fluorescence lifetimes. Considering pristine pyrene (**19**) and 1-acetyl pyrene (**7**), for example, we measured values of 260 ns and ca. 0.15 ns, respectively. This affect parallels that of the fluorescence quantum yields and is ascribed to stem from the n–π* character of the acetyl functionalities. Table 1 documents that all fluorophores − compare **16**–**19** with **3**–**7** − give rise to this trend.

On the other hand, $C_{59}N$ reference **20** shows a mono-exponential decay of its 825 nm fluorescence, for which lifetimes of ca. 1.0 ns were derived in toluene and *o*-dichlorobenzene; this is in good agreement with recent work.[9] Grounds for this fast decay is obtained from the fact that an efficient spin-orbit coupling accelerates the spin-forbidden transition between the singlet and triplet manifolds.

In the corresponding fluorophore-heterofullerene conjugates **10**–**14** evidence for both emissions were found. The fluorophore lifetimes are reduced to about hundred picoseconds and thereby appreciably shortened relative to that seen for **16**–**19**. The underlying lifetimes indicate slower energy transfer rates than found in C_{60}-based arrays, which bear arene-, oligomer-, or porphyrin chromophores as excited-state energy donors.[5] A likely rationale can be seen in the very large energy gap between the singlet excited-state energies of the donor (i.e. 3.0–3.5 eV)[13] and that of the $C_{59}N$ acceptor (1.5 eV). Consequently, it is safe to assume that the overlap integral between the orbitals involved must be small. It is important to note that, in line with the

nearly quantitative $C_{59}N$ fluorescence quantum yields, the fluorescence lifetimes of the $C_{59}N$ moieties in the fluorophore-heterofullerene conjugates **10**–**14** resemble those of $C_{59}N$ reference **20** and are not noticeably impacted by the presence of the fluorophore.[11b] They vary typically between 1.0 and 1.2 ns.

Transient Absorption Measurements

In order to complement the fluorescence studies, the photophysics of **3**–**7**, **10**–**15**, **16**–**19** and **20** were probed by means of time-resolved transient absorption spectroscopy. Following short, pico- (18 ps) and long, nanosecond (8 ns) excitation helps in the analysis of the dynamic processes, which are associated with the generation and fate of the photoexcited states in **3**–**7**, **10**–**15**, **16**–**19** and **20**, and in the identification of the corresponding photoproducts.

In picosecond experiments with **16**–**19** differential absorption changes in the visible and near-infrared region reveal several transient maxima and minima. For example, the singlet–singlet characteristics of pristine pyrene (**19**) are an absorption band in the spectral region around 480–550 nm. None of the fluorophores used show significant singlet deactivations on the picosecond time scale (i.e. up to 4000 ps). The slow intersystem crossing rates in **16**–**19** were tested with nanosecond experiments, which also enabled us to follow the triplet decays (see Table 1).

In **3**–**7**, however, the picosecond domain is dominated by a rapid singlet excited-state deactivation, which takes place nearly instantaneously, that is, close to our time-resolution (i.e. 20 ps). The underlying rates (i.e. $\approx 10^{10}$ s^{-1}) are reasonable matches to the fluorescence lifetimes and corroborate the short-lived nature of photoexcited **3**–**7**. As far as the nanosecond experiments are concerned, the characteristic triplet maxima were employed to determine the triplet lifetimes (Figure 11). Principally, the decay of the triplet excited states of **3**–**7** follows mono-exponential kinetics to recover the singlet ground state. The triplet deactivation is in some cases as fast as 0.5 μs, for example, in acetophenone (**3**), but in 1-acetyl pyrene (**7**) and 2-acetly phenanthrene (**5**) values of 15 μs were found, indicating a notably slower decay.

Differential absorption spectra of $C_{59}N$ reference **20** in toluene solution reveal the growth of a near-infrared absorption maximum, which is centered around 940 nm (not shown).[11b] Principally, this observation is in close agreement with that noted for fullerenes in general, that exhibit singlet–singlet absorptions with a strong near-infrared maximum.[6g] In the case of **20**, this transient absorption is short-lived and decreases through a clean first-order decay (1.1×10^9 s^{-1}). Analogous with this deactivation, the formation of a new absorption develops around 860 nm, similar to that displayed in Figure 12.

The close resemblance of the decay and growth kinetics leads to the conclusion that the underlying process is a direct transformation of the singlet excited state into the energetically lower lying triplet excited state via a spin-forbidden intersystem crossing (*ISC*) between the two manifolds. In the absence of alternative deactivation processes, the triplet lifetime is in the order of 15 μs under our conditions. The product of the spin-forbidden deactivation is the singlet ground state.

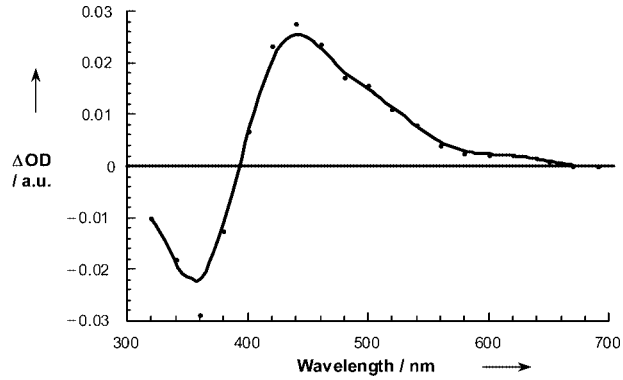

Figure 11. Differential absorption spectrum (visible and near-infrared) obtained upon nanosecond flash photolysis (337 nm) of ca. 1.0×10^{-5} M solutions of 1-acetyl pyrene (**7**) in nitrogen-saturated toluene with a time delay of 50 ns at room temperature.

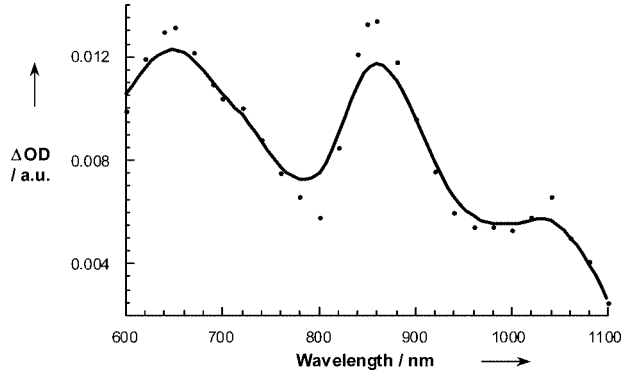

Figure 12. Differential absorption spectrum (visible and near-infrared) obtained upon nanosecond flash photolysis (337 nm) of ca. 1.0×10^{-5} M solutions of **20** in nitrogen-saturated toluene with a time delay of 50 ns at room temperature.

Differential absorption changes, upon picosecond excitation of **10**–**14**, show the singlet excited-state signature of the fluorophore at low time scales (i.e. 20–50 ps). For example, the pyrene singlet excited state in **14** was identified by a transient maximum at ca. 500 nm. However, the fluorophore's lifetime is short: on average, the lifetime of the fluorophores is about 100 ps and, thus matching their fluorescence lifetimes. On a time scale greater than 100 ps, the newly formed singlet excited state of the $C_{59}N$ core is metastable. Similar to the findings on the reference compound, the singlet excited-state features, that is, a broad maximum at ca. 940 nm, undergoes an intramolecular decay, for which we determined rate constants of 1.0×10^9 s^{-1}. The product of this *ISC* is the energetically low-lying triplet excited state.

In line with the proposed energy-transfer mechanism, the differential absorption changes, recorded immediately after an 8-ns pulse, show the same spectral features of the $C_{59}N$ reference triplet excited state as those observed at the end of the picosecond experiments. Precisely, three maxima located at 650, 860, and 1040 nm were observed (Figure 12).

The lifetime of the fullerene triplet was estimated to be ca. 15 μs.

In order to probe the reactivity of the product from photoexcitation of the fluorophore-heterofullerene conjugates **10**–**14**, bimolecular quenching rate constants with molecular oxygen were determined from toluene solutions purged with variable amounts of O_2. The oxygen quenching rate constants ($\approx 10^9$ M^{-1} s^{-1}) are very similar to those noted for pristine fullerenes and monofunctionalized fullerene derivatives.[6]

Conclusion

A series of fluorophore-heterofullerene conjugates **10**–**14** was synthesized in which the flexibility allows an efficient π–π stacking interaction between the chromophores. Photophysical steady-state and time-resolved measurements clearly show the photosensitization effect of the fluorophores that act as an antenna system and transmit their excited-state energy to the covalently attached $C_{59}N$ moiety. This enables the efficient $C_{59}N$ triplet generation, even in a wavelength region where the fullerene absorption is comparatively weak. The overall triplet quantum yields in toluene and *o*-dichlorobenzene are nearly identical with that found for the reference compound. Considering these values, our assignment of an efficient singlet–singlet energy-transfer mechanism controlling the deactivation of the photoexcited fluorophore in fluorophore-heterofullerene conjugates **10**–**14** is unmistakably confirmed.

Experimental Section

Photophysics

Picosecond laser flash photolysis experiments were carried out with 355-nm laser pulses from a mode-locked, Q-switched Quantel YG-501 DP Nd:YAG laser system (pulse width 18 ps, 2–3 mJ/pulse). Nanosecond laser studies were performed with laser pulses from a Molectron UV-400 nitrogen laser system (337.1 nm, 8 ns pulse width, 1 mJ/pulse). The photomultiplier output was digitized with a Tektronix 7912 AD programmable digitizer.

Fluorescence lifetimes were measured with a Laser Strope Fluorescence Lifetime Spectrometer (Photon Technology International) with 337-nm laser pulses from a nitrogen laser fiber-coupled to a lens-based T-formal sample compartment equipped with a stroboscopic detector. Details of the Laser Strobe systems are described on the manufacturer's web site, http://www.pti-nj.com.

Emission spectra were recorded with a SLM 8100 Spectrofluorometer. The experiments were performed at room temperature. Each spectrum represents an average of at least 5 individual scans, and appropriate corrections were applied whenever necessary.

General Remarks and Materials

$(C_{59}N)_2$ (**1**) was prepared according to literature procedures.[7a] ^1H and ^{13}C NMR spectra were obtained with JEOL JNM EX and JEOL JNM GX instruments. Mass spectrometric data were obtained on a Varian MAT 311 A mass spectrometer. UV/Vis spectra were recorded with a Shimadzu UV-3102 spectrometer. IR spectra were obtained with a Bruker Vektor 22 instrument. HPLC analyses were carried out on a Cosmosil Buckyprep Waters column (250×4.6 mm) with toluene as eluent. Acetyl arenes **3**–**7** were bought from Aldrich and used without further purification. In the recently published results[11a] on molecular satellite dishes, 1-(hydroazafullerenyl)pyrene (**2**) has only been briefly mentioned, we therefore describe the synthesis and spectroscopic properties of this compound in this context.

General Experimental Procedure

$(C_{59}N)_2$ (**1**) [60 μmol] and *p*-TsOH were dissolved in ODCB (20 mL). The corresponding amount (see below) of the acetyl compound (pyrene in the case of **2**) was added to this solution. The reaction mixture was heated to 150 °C while a constant stream of air was passed through the solution until all of the $(C_{59}N)_2$ (**1**) was converted into the corresponding heterofullerene-fluorophore conjugate. The reaction was monitored by TLC (silica gel, toluene/ethyl acetate, 9:1). *p*-TsOH was removed by flash chromatography with toluene as eluent. The purification of the heterofullerene adducts was carried out by preparative HPLC using a Cosmosil Buckyprep column with toluene as eluent [1-(admantyl)-2-(hydrazafullerenyl)ethanone (**15**) was isolated without HPLC purification]. The products were precipitated from CS_2/pentane, washed three times with pentane and dried under high vacuum.

1-(Hydroazafullerenyl)-pyrene (2): Pyrene (5 equiv.), *p*-TsOH (15 equiv.). Yield: 11.8 mg, 18%. IR (KBr): $\tilde{\nu}$ = 3037, 2957, 2851, 1735, 1637, 1582, 1547, 1508, 1459, 1422, 1384, 1315, 1288, 1261, 1247, 1214, 1184, 1091, 1033, 962, 906, 843, 810, 759, 711, 683, 613, 578, 567, 555, 524, 480, 470 cm^{-1}. UV/Vis (ODCB): λ_{max} = 323, 337, 354, 442, 588, 717 nm. ^1H NMR (CS_2/$CDCl_3$, 400 MHz): δ = 10.53 (d, ^3J = 9.4 Hz, 1 H), 9.54 (d, ^3J = 8.2 Hz, 1 H), 8.57 (d, ^3J = 8.2 Hz, 1 H), 8.51 (d, ^3J = 9.4 Hz, 1 H), 8.37 (d, ^3J = 7.5 Hz, 1 H), 8.32 (d, ^3J = 7.5 Hz, 1 H), 8.26 (s, 2 H), 8.14 (t, ^3J = 7.5 Hz, 1 H) ppm. ^{13}C NMR (CS_2/$CDCl_3$, 100.4 MHz): δ = 154.53 (2 C), 149.03 (2 C), 147.49 (1 C), 147.34 (2 C), 147.09 (2 C), 146.79 (2 C), 146.45 (2 C), 146.33 (2 C), 146.17 (2 C), 146.01 (2 C), 145.67 (2 C), 145.60 (1 C), 145.47 (2 C), 144.95 (2 C), 144.92 (2 C), 144.38 (2 C), 144.26 (2 C), 143.77 (2 C), 143.05 (2 C), 142.68 (2 C), 142.00 (2 C), 141.80 (2 C), 141.29 (2 C), 141.08 (2 C), 140.97 (2 C), 140.84 (2 C), 139.50 (2 C), 137.05 (2 C), 134.91 (2 C), 133.18 (1 C, ar), 132.65 (1 C, ar), 131.25 (1 C, ar), 130.60 (1 C, ar), 130.35 (1 C, ar), 128.96 (1 C, ar), 128.85 (1 C, ar), 128.60 (1 C, ar), 127.26 (1 C, ar), 126.38 (1 C, ar), 126.12 (1 C, ar), 126.05 (1 C, ar), 125.94 (1 C, ar), 125.19 (1 C, ar), 124.87 (2 C), 124.57 (1 C, ar), 124.21 (1 C, ar), 84.61 (1 C, C-sp^3) ppm. MS (EI): *m*/*z* = 924 $[M]^+$, 722 $[C_{59}N]^+$.

2-(Hydroazafullerenyl)-1-(adamant-2-yl)ethanone (15): 1-Acetyladamantane (15 equiv.), *p*-TsOH (30 equiv.). Yield: 33.7 mg, 55%. IR (KBr): $\tilde{\nu}$ = 2900, 2846, 1703, 1636, 1582, 1550, 1510, 1448, 1423, 1343, 1315, 1291, 1238, 1214, 1196, 1186, 1143, 1108, 1092, 1047, 1010, 970, 931, 842, 809, 766, 745, 733, 720, 669, 648, 578, 568, 556, 524, 503, 480, 468, 420 cm^{-1}. UV/Vis (ODCB): λ_{max} = 323, 447, 597, 730, 794 nm. ^1H NMR (CS_2/$CDCl_3$, 400 MHz): δ = 4.91 (s, 2 H), 2.28 (s, 9 H), 1.94 (s, 6 H) ppm. ^{13}C NMR (CS_2/$CDCl_3$, 100.4 MHz): δ = 209.16 (1 C, CO), 155.04 (2 C), 148.88 (2 C), 147.57 (1 C), 147.36 (2 C), 147.04 (2 C), 146.96 (2 C), 146.87 (2 C), 146.34 (2 C), 146.25 (2 C), 145.97 (2 C), 145.73 (2 C), 145.54 (1 C), 145.44 (2 C), 144.84 (2 C), 144.72 (2 C), 144.09 (2 C), 144.03 (2 C), 143.77 (2 C), 142.82 (2 C), 142.53 (2 C), 141.81 (2 C), 141.51 (2 C), 141.15 (2 C), 141.04 (2 C), 140.76 (2 C), 140.74 (2 C), 139.32 (2 C), 137.40 (2 C), 134.41 (2 C), 124.81 (2 C), 78.67 (1 C, C-sp^3), 47.04 (1 C), 46.97 (1 C), 38.40 (3 C), 36.71 (3 C), 28.41 (3 C) ppm. MS (EI): *m*/*z* = 899 $[M]^+$, 766 $[C_{59}N]^+$ + [–CH_2CO–], 722$[C_{59}N]^+$.

2-(Hydroazafullerenyl)-1-(naphthalen-1-yl)ethanone (11): 2-Acetylnaphthalene (20 equiv.), *p*-TsOH (40 equiv.). Yield: 19.5 mg, 31%.

IR (KBr): $\tilde{\nu}$ = 3045, 2925, 2900, 2846, 1690, 1618, 1583, 1550, 1510, 1459, 1421, 1384, 1343, 1315, 1291, 1230, 1214, 1196, 1175, 1141, 1092, 1027, 1008, 950, 890, 842, 809, 766, 744, 720, 672, 651, 580, 568, 556, 524, 503, 480, 468, 420 cm^{-1}. UV/Vis (ODCB): λ_{max} = 320, 446, 597, 730, 794 nm. ^1H NMR ($CS_2/CDCl_3$, 400 MHz): δ = 8.96 (s, 1 H), 8.43 (d, ^3J = 8.5 Hz, 1 H,), 8.12 (d, ^3J = 7.7 Hz, 1 H), 8.07 (d, ^3J = 8.5 Hz, 1 H), 7.97 (d, ^3J = 7.9 Hz, 1 H), 7.66 (m, 2 H), 5.59 (s, 2 H, CH_2) ppm. ^{13}C NMR ($CS_2/CDCl_3$, 100.4 MHz): δ = 193.96 (1 C, CO), 155.07 (2 C), 148.67 (2 C), 147.59 (1 C), 147.39 (2 C), 147.12 (2 C), 146.97 (2 C), 146.92 (2 C), 146.36 (2 C), 146.29 (2 C), 145.99 (2 C), 145.75 (2 C), 145.57 (1 C), 145.47 (2 C), 144.87 (2 C), 144.75 (2 C), 144.11 (2 C), 143.80 (2 C), 142.87 (2 C), 142.56 (2 C), 141.85 (2 C), 141.55 (2 C), 141.20 (2 C), 141.07 (2 C), 140.83 (2 C), 140.77 (2 C), 139.42 (2 C), 137.45 (2 C), 135.70 (1 C, ar), 134.55 (2 C), 133.99 (1 C, ar), 132.38 (1 C, ar), 130.17 (1 C, ar), 129.57 (1 C, ar), 128.80 (1 C, ar), 128.77 (1 C, ar), 127.80 (1 C, ar), 126.95 (1 C, ar), 124.81 (2 C), 123.81 (1 C, ar), 78.74 (1 C, C-sp^3), 49.56 (1 C, CH_2) ppm. MS (EI): *m/z* = 892 $[M]^+$, 766 $(C_{59}N)^+$ + [–CH_2CO–], 722 $[C_{59}N]^+$.

2-(Hydroazafullerenyl)-1-(phenanthren-2-yl)ethanone (12): 2-Acetylphenantrene (30 equiv.), *p*-TsOH (30 equiv.). Yield: 9.4 mg, 14%. IR (KBr): $\tilde{\nu}$ = 3048, 2998, 2921, 2851, 1685, 1618, 1594, 1569, 1549, 1509, 1459, 1421, 1384, 1343, 1316, 1290, 1228, 1197, 1172, 1141, 1092, 1007, 1000, 946, 882, 863, 830, 807, 767, 744, 719, 707, 689, 672, 651, 622, 580, 567, 556, 541, 523, 503, 482, 469, 453, 422 cm^{-1}. UV/Vis (ODCB): λ_{max} = 316, 445, 594, 728, 793 nm. ^1H NMR ($CS_2/CDCl_3$, 400 MHz): δ = 8.96 (d, ^4J = 1.9 Hz, 1 H), 8.90 (d, ^3J = 8.8 Hz, 1 H), 8.76 (d, ^3J = 8.5 Hz, 1 H), 8.63 (dd, ^3J = 8.8, ^4J = 1.9 Hz, 1 H), 7.97 (m, 2 H), 7.88 (d, ^3J = 8.5 Hz, 1 H), 7.72 (m, 2 H), 5.62 (s, 2 H, CH_2) ppm. ^{13}C NMR ($CS_2/CDCl_3$, 100.4 MHz): δ = 193.72 (1 C, CO), 155.04 (2 C), 148.64 (2 C), 147.58 (1 C), 147.38 (2 C), 147.12 (2 C), 146.97 (2 C), 146.91 (2 C), 146.35 (2 C), 146.28 (2 C), 145.99 (2 C), 145.74 (2 C), 145.55 (1 C), 145.46 (2 C), 144.86 (2 C), 144.73 (2 C), 144.11 (4 C), 143.79 (2 C), 142.86 (2 C), 142.55 (2 C), 141.84 (2 C), 141.55 (2 C), 141.20 (2 C), 141.06 (2 C), 140.82 (2 C), 140.76 (2 C), 139.42 (2 C), 137.44 (2 C), 134.54 (1 C, ar), 134.37 (2 C), 133.67 (1 C, ar), 132.88 (1 C, ar), 131.40 (1 C, ar), 129.81 (1 C, ar), 129.40 (1 C, ar), 128.63 (1 C, ar), 128.22 (1 C, ar), 127.89 (1 C, ar), 127.16 (1 C, ar), 127.00 (1 C, ar), 124.97 (1 C, ar), 124.81 (2 C), 123.44 (1 C, ar), 123.18 (1 C, ar), 78.74 (1 C, C-sp^3), 49.62 (1 C, CH_2) ppm. MS (EI): *m/z* = 941 $[M]^+$, 722 $[C_{59}N]^+$.

2-(Hydroazafullerenyl)-1-(9*H*-fluoren-2-yl)ethanone (13): 2-Acetylfluorene (15 equiv.), *p*-TsOH (30 equiv.). Yield: 19.2 mg, 30%. IR (KBr): $\tilde{\nu}$ = 2998, 2922, 2852, 1682, 1607, 1566, 1550, 1511, 1458, 1422, 1396, 1343, 1246, 1216, 1197, 1186, 1130, 1116, 1093, 1045, 949, 835, 768, 732, 678, 645, 579, 568, 556, 524, 481, 469 cm^{-1}. UV/Vis (ODCB): λ_{max} = 319, 442, 558, 592, 722, 809 nm. ^1H NMR ($CS_2/CDCl_3$, 400 MHz): δ = 8.59 (d, ^4J = 0.8 Hz, 1 H), 8.48 (dd, ^3J = 8.0, ^4J = 1.4 Hz, 1 H), 8.01 (d, ^3J = 8.0 Hz, 1 H), 7.89 (dd, ^3J = 6.9, ^4J = 1.4 Hz, 1 H), 7.62 (d, ^3J = 6.2 Hz 1 H), 7.42 (m, 2 H), 5.52 (s, 2 H, CH_2), 4.11 (s, 2 H, CH_2) ppm. ^{13}C NMR ($CS_2/CDCl_3$, 100.4 MHz): δ = 193.70 (1 C, CO), 155.08 (2 C), 148.78 (2 C), 147.60 (1 C), 147.40 (2 C), 147.12 (2 C), 147.02 (2 C), 146.99 (1 C, ar), 146.94 (2 C), 146.37 (2 C), 146.30 (2 C), 146.00 (2 C), 145.77 (2 C), 145.58 (1 C), 145.48 (2 C), 144.88 (2 C), 144.76 (2 C), 144.19 (1 C, ar), 144.12 (4 C), 143.81 (2 C), 143.37 (1 C, ar), 142.88 (2 C), 142.57 (2 C), 141.86 (2 C), 141.56 (2 C), 141.20 (2 C), 141.09 (2 C), 140.82 (2 C), 140.78 (2 C), 140.06 (1 C, ar), 139.41 (2 C), 137.46 (2 C), 135.06 (1 C, ar), 134.53 (2 C), 128.27 (1 C, ar), 127.80 (1 C, ar), 127.10 (1 C, ar), 125.12 (1 C, ar), 125.00 (1 C, ar), 124.81 (2 C), 120.91 (1 C, ar), 119.88 (1 C, ar), 78.83 (1 C, C-sp^3), 49.61 (1 C, CH_2), 37.00 (1 C, CH_2) ppm. MS (EI): *m/z* = 927 $[M]^+$, 766 $[C_{59}N]^+$ + [–CH_2CO–], 722 $[C_{59}N]^+$.

2-(Hydroazafullerenyl)-1-(pyren-1-yl)ethanone (14): 1-Acetylpyrene (7.5 equiv.), *p*-TsOH (15 equiv.). Yield: 28.1 mg, 42%. IR (KBr): $\tilde{\nu}$ = 3037, 2980, 2920, 2851, 1675, 1623, 1593, 1582, 1550, 1505, 1422, 1382, 1327, 1213, 1186, 1119, 1092, 994, 961, 844, 767, 744, 715, 674, 578, 568, 555, 524, 483, 468, 441 cm^{-1}. UV/Vis (ODCB): λ_{max} = 290, 361, 396, 439, 592, 725, 807 nm. ^1H NMR ($CS_2/CDCl_3$, 400 MHz): δ = 9.51 (d, ^3J = 9.3 Hz, 1 H), 9.00 (d, ^3J = 8.0 Hz, 1 H), 8.39 (d, ^3J = 8.0 Hz, 1 H), 8.33 (d, ^3J = 9.3 Hz, 1 H), 8.27 (m, 3 H), 8.18 (d, ^3J = 8.8 Hz, 1 H), 8.10 (t, ^3J = 7.7 Hz, 1 H), 5.73 (s, 2 H, CH_2) ppm. ^{13}C NMR ($CS_2/CDCl_3$, 100.4 MHz): δ = 197.72 (1 C, CO), 155.09 (2 C), 148.83 (2 C), 147.60 (1 C), 147.40 (2 C), 147.13 (2 C), 147.00 (2 C), 146.95 (2 C), 146.37 (2 C), 146.30 (2 C), 146.00 (2 C), 145.75 (2 C), 145.59 (1 C), 145.48 (2 C), 144.89 (2 C), 144.75 (2 C), 144.13 (4 C), 143.82 (2 C), 142.87 (2 C), 142.56 (2 C), 141.85 (2 C), 141.56 (2 C), 141.23 (2 C), 141.11 (2 C), 140.83 (2 C), 140.76 (2 C), 139.44 (2 C), 137.49 (2 C), 134.51 (1 C, ar), 134.41 (2 C), 130.82 (1 C, ar), 130.66 (1 C, ar), 130.31 (1 C, ar), 130.29 (1 C, ar), 130.28 (1 C, ar), 130.18 (1 C, ar), 130.13 (1 C, ar), 127.24 (1 C, ar), 127.06 (1 C, ar), 126.97 (1 C, ar), 126.58 (1 C, ar), 126.54 (1 C, ar), 126.39 (1 C, ar), 125.19 (1 C, ar), 125.03 (1 C, ar), 124.86 (2 C), 124.02 (1 C, ar), 123.99 (1 C, ar), 79.27 (1 C, C-sp^3), 52.61 (1 C, CH_2) ppm. MS (EI): *m/z* = 965 $[M]^+$, 766 $[C_{59}N]^+$ + [–CH_2CO–], 722 $[C_{59}N]^+$.

Acknowledgments

We thank the SFB 583, "Redoxaktive Metallkomplexe – Reaktivitätssteuerung durch molekulare Architekturen" and the Graduierte-Kolleg "Homogener und Heterogener Elektronentransfer" for financial support. Part of this research was supported by the US Department of Energy. This is contribution NDRL-4594 from the Radiation Laboratory.

[1] J. Deisenhofer, J. R. Norris (Eds.), *The Photosynthetic Reaction Center*, Academic Press, New York, **1993**.
[2] a) F. L. Carter, *Molecular Electronic Devices*, Dekker, New York, **1987**; b) M. A.Fox, M. Channon (Eds.), *Photoinduced Electron Transfer*, Elsevier, Amsterdam, **1988**; c) V. Balzani (Ed.), *Electron Transfer in Chemistry*, Wiley-VCH, Weinheim, **2001**; d) M. D. Newton, *Chem. Rev.* **1991**, *91*, 767; e) M. R. Wasielewski, *Chem. Rev.* **1992**, *92*, 435; f) D. Gust, T. A. Moore, A. L. Moore, *Acc. Chem. Res.* **1993**, *26*, 198; g) M. N. Paddon-Row, *Acc. Chem. Res.* **1994**, *27*, 18; h) I. R. Gould, S. Farid, *Acc. Chem. Res.* **1996**, *29*, 522; i) V. Balzani, A. Juris, M. Venturi, S. Campagna, S. Serroni, *Chem. Rev.* **1996**, *96*, 759; j) I. Willner, *Acc. Chem. Res.* ***1997***, *30*, 347; k) P. Piotrowiak, *Chem. Soc. Rev.* **1999**, *28*, 143; l) H. Kurreck, M. Huber, *Angew. Chem. Int. Ed. Engl.* **1995**, *34*, 849.
[3] P. R. Ogilby, *Singlet Oxygen Organic Molecules and Light*, John Wiley and Sons Ltd, New York, **1994**.
[4] T. Da Ros, M. Prato, *Chem. Commun.* **1999**, 663–669.
[5] a) F. Diederich, R. Kessinger, *Acc. Chem. Res.* **1999**, *32*, 537–545; b) A. Hirsch (Ed.), *Fullerenes and Related Structures, Top. Curr. Chem. vol. 199*, Springer, Berlin, **1999**; c) M. Prato, M. Maggini, *Acc. Chem. Res.* **1998**, *31*, 519–526; d) R. Taylor (Ed.), *Lecture Notes on Fullerenes Chemistry*, Imperial College Press, London, **1999**; e) A. Hirsch, M. Brettreich, *Fullerenes – Chemistry and Reactions*, Wiley-VCH, Weinheim, **2004**.
[6] a) H. Imahori, Y. Sakata, *Adv. Mater.* **1997**, *9*, 537–546; b) M. Prato, *J. Mater. Chem.* **1997**, *7*, 1097–1109; c) N. Martin, L. Sanchez, B. Illescas, I. Perez, *Chem. Rev.* **1998**, *98*, 2527–2547; d) H. Imahori, Y. Sakata, *Eur. J. Org. Chem.* **1999**, 2445–2457;

e) F. Diederich, M. Gomez-Lopez, *Chem. Soc. Rev.* **1999**, *28*, 263–277; f) D. M. Guldi, *Chem. Commun.* **2000**, 321–327; g) D. M. Guldi, M. Prato, *Acc. Chem. Res.* **2000**, *33*, 695–703; h) C. A. Reed, R. D. Bolskar, *Chem. Rev.* **2000**, *100*, 1075–1119; i) D. Gust, T. A. Moore, A. L. Moore, *J. Photochem. & Photobiol. B* **2000**, *58*, 63–71; j) D. Gust, T. A. Moore, A. L. Moore, *Acc. Chem. Res.* **2001**, *34*, 40–48; k) D. M. Guldi, *Chem. Soc. Rev.* **2002**, *31*, 22–36; l) D. M. Guldi, N. Martin, *J. Mater. Chem.* **2002**, *12*, 1978; m) H. Imahori, Y. Mori, Y. Matano, *J. Photochem. Photobiol. C* **2003**, *4*, 51–83; n) J. F. Nierengarten, *Top. Curr. Chem.* **2003**, *228*, 87; o) D. M. Guldi, *Pure Appl. Chem.* **2003**, *75*, 1069; p) M. E. El-Khouly, O. Ito, F. D'Souza, *J. Photochem. Photobiol. C* **2004**, *5*, 79; q) D. M. Guldi, M. Prato, *Chem. Commun.* **2004**, 2517; r) D. M. Guldi, F. Zerbetto, V. Georgakilas, M. Prato, *Acc. Chem. Res.* **2005**, *38*, 38.

[7] a) J. C. Hummelen, B. Knight, J. Pavlovich, R. González, F. Wudl, *Science* **1995**, *269*, 1554–1556; b) B. Nuber, A. Hirsch, *Chem. Commun.* **1996**, 1421–1422.

[8] a) B. Nuber, A. Hirsch, *Chem. Commun.* **1998**, 405–406; b) F. Hauke, A. Hirsch, *Chem. Commun.* **1999**, 2199–2200; c) F. Hauke, A. Hirsch, *Tetrahedron* **2001**, *57*, 3697–3708; d) F. Hauke, A. Hirsch, *Chem. Commun.* **2001**, 1316–1317.

[9] a) M. Keshavarz-K, R. González, R. G. Hicks, G. Srdanov, V. I. Srdanov, T. G. Collins, J. C. Hummelen, C. Bellavia-Lund, J. Pavlovich, F. Wudl, K. Holczer, *Nature* **1996**, *383*, 147–150; b) C. Bellavia-Lund, R. González, J. C. Hummelen, R. G. Hicks, A. Sastre, F. Wudl, *J. Am. Chem. Soc.* **1997**, *119*, 2946–2947; c) A. Gruss, K.-P. Dinse, A. Hirsch, B. Nuber, U. Reuther, *J. Am. Chem. Soc.* **1997**, *119*, 8728–8729; d) C. Bellavia-Lund, M. Keshavarz-K, T. Collins, F. Wudl, *J. Am. Chem. Soc.* **1997**, *119*, 8101–8102; e) J. C. Hummelen, C. Bellavia-Lund, F. Wudl, *Top. Curr. Chem.* **1999**, 199, 93–134; f) B. Nuber, A. Hirsch, *Acc. Chem. Res.* **1999**, *32*, 795–804; g) U. Reuther, A. Hirsch, *Carbon* **2000**, *38*, 1539–1549; h) D. M. Guldi, F. Hauke, A. Hirsch, *Res. Chem. Intermed.* **2002**, *28*, 817–830.

[10] K.-C. Kim, F. Hauke, A. Hirsch, P. D. W. Boyd, E. Carter, R. S. Armstrong, P. A. Lay, Ch. A. Reed, *J. Am. Chem. Soc.* **2003**, *125,* 4024–4025.

[11] a) F. Hauke, S. Atalick, D. M. Guldi, J. Mack, L. T. Scott, A. Hirsch, *Chem. Commun.* **2004**, 766–767; b) F. Hauke, A. Hirsch, S.-G. Liu, L. Echegoyen, A. Swartz, C. Luo, D. M. Guldi, *ChemPhysChem* **2002**, *3*, 195.

[12] *PC Spartan Pro*, Molecular Modelling Package, Wavefunction Inc., Irvine, Ca., USA:

[13] S. L. Murov, I. Carmichael, G. L. Hug, *Handbook of Photochemistry*, Marcel Dekker, New York, **1993**.

[14] A better solvation of the radical ion pairs in the polar solvents lowers the energy of the charge-separated state, while the excited-state energies remain virtually unchanged.

Received: October 27, 2004
Published Online: March 8, 2005

